Control of Whispering Gallery Modes and PT-symmetry Breaking in Colloidal Quantum Dot Microdisk Lasers with Engineered Notches

Qingji Zeng¹, Evan Lafalce¹, ChunHao Lin², Marcus J. Smith^{2,3}, Jaehan Jung², Young Yoon², Zhiqun Lin², Vladimir V. Tsukruk², Z. Valy Vardeny¹

Abstract

Whispering gallery mode resonators have been demonstrated to be a great way to achieve superior optical cavities with high quality factor and small mode volume. However due to the high sensitivity of these modes to the properties of the resonator boundary, they are susceptible to parasitic splitting of clockwise and counter-clockwise modes. In this work, we investigate the effect of implantation of an engineered notch into the boundary of a circular microdisk resonator fabricated from colloidal quantum dots, which are particularly sensitive to boundary defects. We observed a strong reduction of parasitic mode splitting with introduction of a large engineered notch, as well as enhanced directionality of laser emission. We further investigate the performance of these resonators in evanescently coupled pairs, where the modal interaction allows modulation of laser behavior through variation of the gain and loss induced by the optical pump. We show that two distinct cases of modal interaction can be achieved by adjusting the size of the engineered notch, providing a bridge between intra- and inter-disk modal interactions for laser spectral control.

Keywords

Quantum dot, microlaser, whispering-gallery mode, exceptional point

¹Department of Physics & Astronomy, University of Utah, Salt Lake City, UT. 84112, USA ²School of Materials Science and Engineering, Georgia Institute of Technology, Atlanta, GA. 30332, USA

³Aerospace Systems Directorate, Air Force Research Laboratory, Wright-Patterson Air Force Base, Ohio 45433, USA

Introduction

One of the main goals in the development of laser cavity configurations is to achieve high quality factor (Q), small mode volume (V), and small volume resonant cavities¹. Large Q/V may result in strong coupling between the cavity field and active material, which promotes low threshold and narrow linewidth lasers^{2,3}. Whispering gallery mode (WGM) resonators have been realized to be an efficient way to achieve high Q/V, because of total internal reflection at the dielectric/environment boundary ⁴. A large number of cavity structures have been fabricated to support WGMs with high Q factors including microspheres⁵, microtoroids⁶, and microdisks⁷. These WGM resonators have proven beneficial in applications ranging from low-threshold lasers², to environmental and particle sensors⁸ and optical frequency combs⁹. Further potential exists in the ability to link these resonators in arrays, as nicely demonstrated in the construction of topological photonic lasers¹⁰.

Since their realization, a significant focus of research on WGM lasers has been the ability to control the directionality of light out-coupling. This is a challenge because the high-confinement that makes these devices so beneficial provides near unity reflection at the boundary, and hence out-coupling only occurs isotopically through evanescent leaking at the boundary walls. Approaches to impart directionality have taken the form of perturbation of the boundary either by global deformation into non-circular geometry or a localized disturbance¹¹⁻¹⁶. Such studies have shown promising achievement in laser directional output. However, less attention has been given to the ability to control the spectral properties of WGM lasers by boundary deformations. This is particularly important for semiconductor lasers with large gain bandwidth that support multi-modal emission even for small cavity dimensions. Obtaining spectral purity in such lasers may be difficult, requiring high precision or greater complexity in the cavity design. Engineering stable spectral purity of multi-mode resonators is important for applications such as nanoparticle or environment sensing, where the frequency splitting of clockwise and anticlockwise modes is used to detect external particles, which would be rendered ineffective if the unperturbed cavity suffered from parasitic mode splitting. Additionally, the presence of broadband regularly spaced lines is necessary for optical frequency comb spectroscopy.

Laser materials systems such as colloidal quantum dots (CQDs) that lend to easier fabrication for on-chip photonic modules and laser arrays are being intensively pursued¹⁷⁻²⁸. A great benefit of CQDs is the ability to choose emission wavelength by choice of the quantum dot size or chemical composition. These materials also possess high optical gains for low-threshold lasing which can reduce the power consumption of such modules while maintaining high-throughput processing and size-scalability. In this work, we investigate the effect of implantation of an engineered notch into the boundary of circular microdisk resonators fabricated from a hybrid microfabrication and solution-based, size-scalable process based on colloidal quantum dots. As we previously reported, in such resonators, parasitic mode-splitting in the laser emission spectrum becomes an issue^{18,29}. Through the introduction of a large engineered notch, we observe a strong and consistent reduction of mode splitting, as well as enhanced directionality of the laser emission.

Meanwhile, the recent development of non-Hermitian and Parity-Time symmetric optics and photonics^{30,31} has relied heavily on the capabilities of WGM resonators. Through judicious control of optical properties such as refractive index, gain and loss, and modal coupling, these systems exploit the physics of exceptional points and subsequently achieve intriguing behavior such as single-mode lasing^{32,33}, chiral modes³⁴, and orbital angular momentum beams³⁵. The ability to chemically tailor the optical properties of CQDs makes them very attractive for applications in this field. Here, we further exploit the ability to control the spectral purity through the intra-cavity interaction resulting from the engineered notch to provide a wider range of achievable behavior in evanescently coupled pairs, where the modal interaction allows modulation of laser behavior through deliberate spatial distribution of the externally applied gain and loss.

Results & Discussion

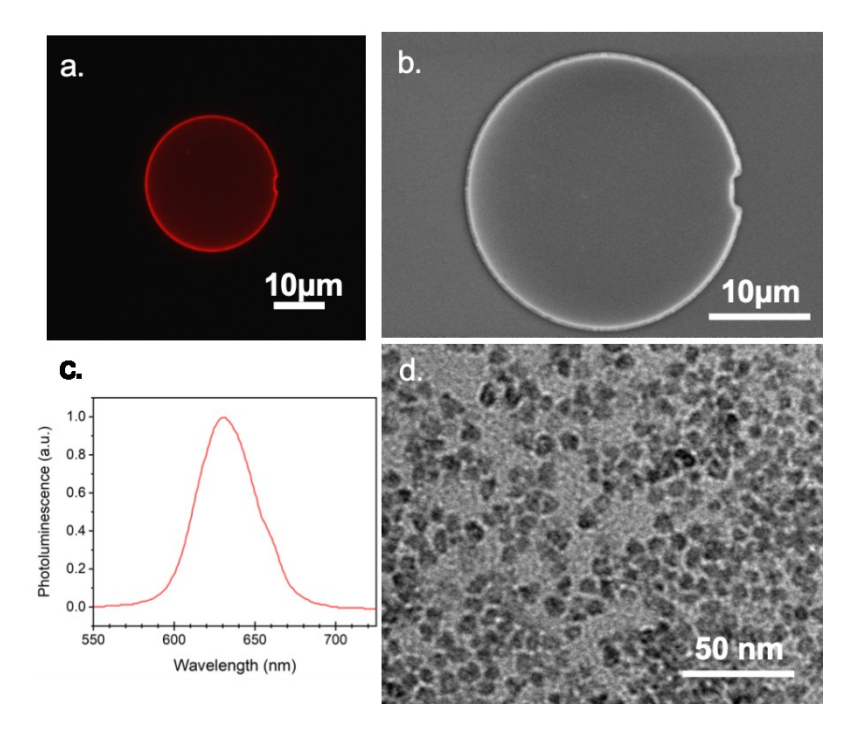


Figure 1. Characterization of Engineered Notch Microdisks and Quantum Dots. a. 50x PL image of individual microdisk with engineered notch. b. SEM image of individual microdisk with engineered notch. c. PL spectrum of colloidal QDs used to fabricate the microdisk d. TEM of crosslinked QDs that shows uniform size distribution and close packing.

For our study, we developed lasing systems based on high-optical gain, core/alloyed shell-CdSe/Cd_{1-x}Zn_xSe_{1-y}S_y colloidal quantum dots (CQD) produced from a one-pot synthesis. The large size $(7.5 \pm 0.8 \text{ nm})$ and compositional gradient shell reduce Auger recombination and provides low-threshold for laser action^{18,36-38}. Circular microdisk CQD laser cavities were then fabricated using a hybrid bottom-up/top-down approach in which a photoresist was lithographically patterned with trenches for precise spatial position and size control microdisk arrays, whereupon the microdisks were built up by a layer-by-layer deposition of CQDs and ligand cross-linking treatment (see Methods and Supplemental Figures S1-2 for more details). This

procedure was used to produce microcavities of $26~\mu$ m diameter and 100 nm thickness. Furthermore, the lithographic fabrication allows for incorporation of an 'engineered notch' boundary deformation in the circular perimeter. The circumferential arc length of these notches is 3100 ± 500 nm whereas the radial depth of the notch, d, is systematically varied between 0 and 1000 nm. Such engineered notches allow for advantageous control of laser modes as described below.

Microdisks were optically pumped with 532 nm pulsed laser of temporal pulse width of 7 ps and 200 Hz repetition rate. Figure 2a shows the emission spectrum of a microdisk with the largest notch size ($d = 1050 \pm 50$ nm) when pumped at different intensities. At low pump fluence, that is below the lasing threshold, there is only broad spontaneous emission. As the pump fluence is increased, a series of equally spaced narrow modes emerge once the optical gain overcomes the intrinsic loss at threshold and laser modes are generated in the cavity. These narrow modes show constant free spectral range, $\Delta \lambda = \lambda^2/n_{\rm eff}(\pi D)$ which is 2.6 \pm 0.2 nm, where the D is the disk diameter (D = $26 \pm 0.1 \mu m$). From these parameters, we can get the effective mode index of refraction, $n_{eff} = 1.85 \pm 0.05$, which matches the refractive index of CdSe/Cd_{1-x}Zn_xSe_{1-y}S_y (n = 1.86 \pm 0.05) that was determined by ellipsometry^{37,38}. The mode spacing is equal to that of a pristine microdisk without a notch (d = 0 nm) within the experimental uncertainty, which means that the notch does not affect the free spectral range. This is shown clearly in the comparison of the Fourier transform between normal disk and the notched disk shown in Fig. 2b. The emission intensity vs. pump intensity of the two kinds of disk structures are shown in Fig. 2c. We find that the lasing threshold of the notch disk is around 66.5 $\mu J/cm^2$ which is higher than that of the pristine disk $(27.5 \,\mu\text{J/cm}^2)$ as well as the threshold for amplified spontaneous emission of unpatterened CQD film (Supplemental Figure S3); this is caused by the overall loss added to the modes by the presence of the notch. In addition to the lasing threshold, the directional properties of the laser emission are also significantly influenced by the notch. The emission power measured as function of azimuthal angle in the plane of the disk is shown in Fig. 2d. The emission at the opposite direction of the notch is strongly enhanced. The engineered notch acts as a large scatterer which channels light to a unique direction (opposite from the notch position); this phenomenon has been previously used to generate a highly unidirectional WGM laser¹⁶.

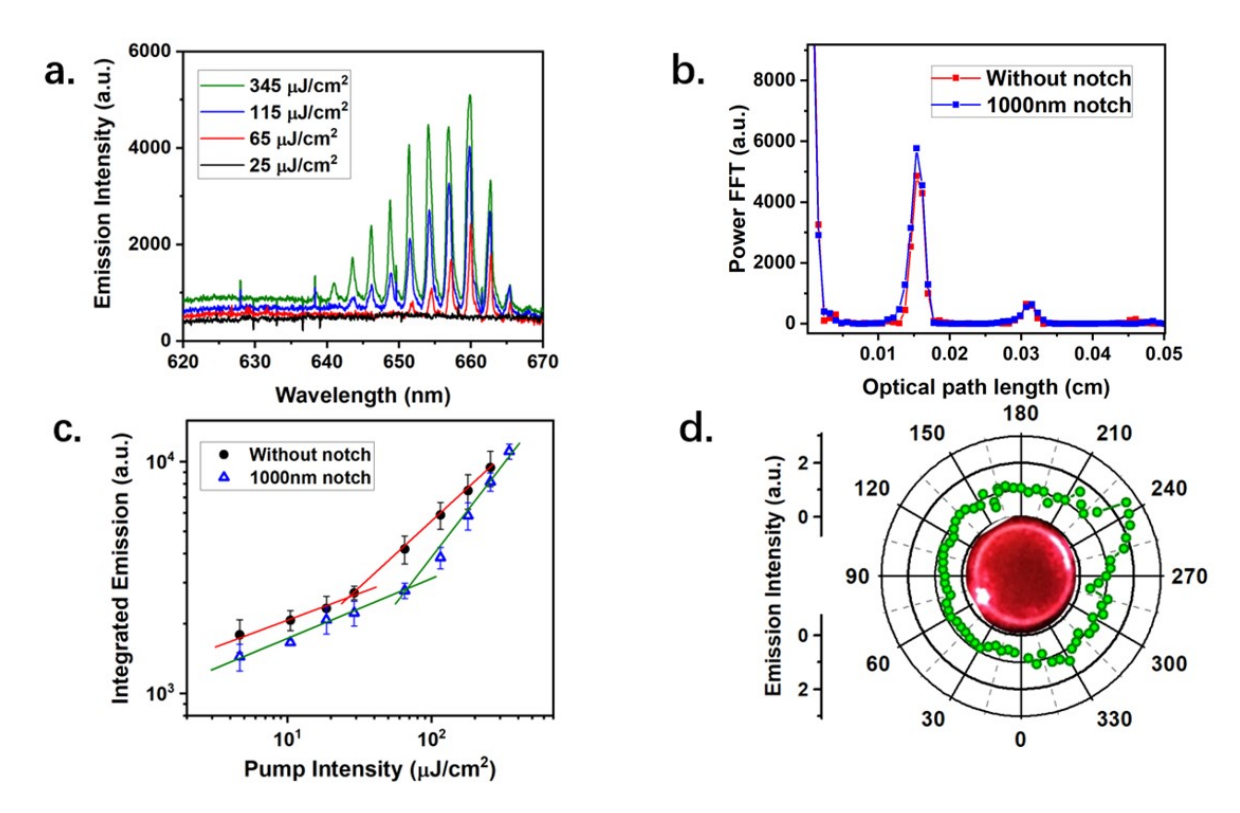


Figure 2. Lasing properties of a microdisk with engineered notch of 1000nm depth. a. Emission spectrum of microdisk laser with notch at various pump intensities as indicated. b. Fourier transform of the emission spectrum for a pristine microdisk and engineered notch microdisk. c. Emission intensity vs. pump intensity of pristine microdisk and microdisk with notch. The straight lines denote the asymptotes below and above threshold, respectively. d. Angular dependence of the laser emission intensity of an engineered notch microdisk with fluorescent image inset in the center. The notch is positioned at 60 degrees.

More strikingly, we find that the spectral properties of WGM are strongly influenced by the notch depth, d. Fig. 3a shows the emission spectrum from a microdisk without an engineered notch (d = 0 nm). It is clear that there is an additional set of modes with the same free spectral range, as a result of mode splitting. As we have previously reported²⁴, asymmetric scattering caused by structural perturbation along the circumference results in breaking of degeneracy between clockwise (CW) and counter-clockwise (CCW) propagating modes and the observation of mode splitting. The perturbations in this case occur naturally with varying frequency as a result of the fabrication process. In order to characterize the mode splitting between samples, we use an empirical parameter ϕ^{λ} to quantify the splitting between individual broken-degeneracy WGM mode-pairs,

$$\phi^{\lambda} = \frac{2|\lambda_1 - \lambda_2|}{\Lambda \lambda} \tag{1}$$

Where λ_1 and λ_2 are the peak wavelengths of the two modes and $\Delta\lambda$ is the free spectral range. We then take the average of the splitting parameter across all the modes in the spectrum of a microdisk $\langle \phi^{\lambda} \rangle = \sum_{i}^{N} \phi_{i}^{\lambda}$. We measured a large number of microdisks and obtained a distribution of the splitting for each notch depth. Fig. 3b shows the splitting parameter distribution of normal

microdisks (d = 0 nm). We can see that there is a large ratio of microdisks with high splitting parameter values. The splitting in this case results from perturbation introduced by fabrication defects^{18,29}. The emission spectra of microdisk with an engineered small notch (d < 450 nm) also shows similar mode splitting as demonstrated in the representative example in Fig. 3c. For this range of notch depths, we see that the splitting parameter more consistently takes high values due to the controlled implantation of the engineered notch (Fig. 3d). As the notch depth is increased further, above 450 nm, then the mode splitting of CW and CCW propagating modes is not observed since only one set of modes appears in the spectrum (see Fig. 3e). The spitting parameter distribution, shown in Fig. 3f clearly demonstrates that the large notch depth produces emission spectra free from mode-splitting with high regularity. We summarized the relation of splitting parameter as a function of the engineered notch depth in Fig. 4a, which shows the splitting parameter averaged over several samples at each notch depth.

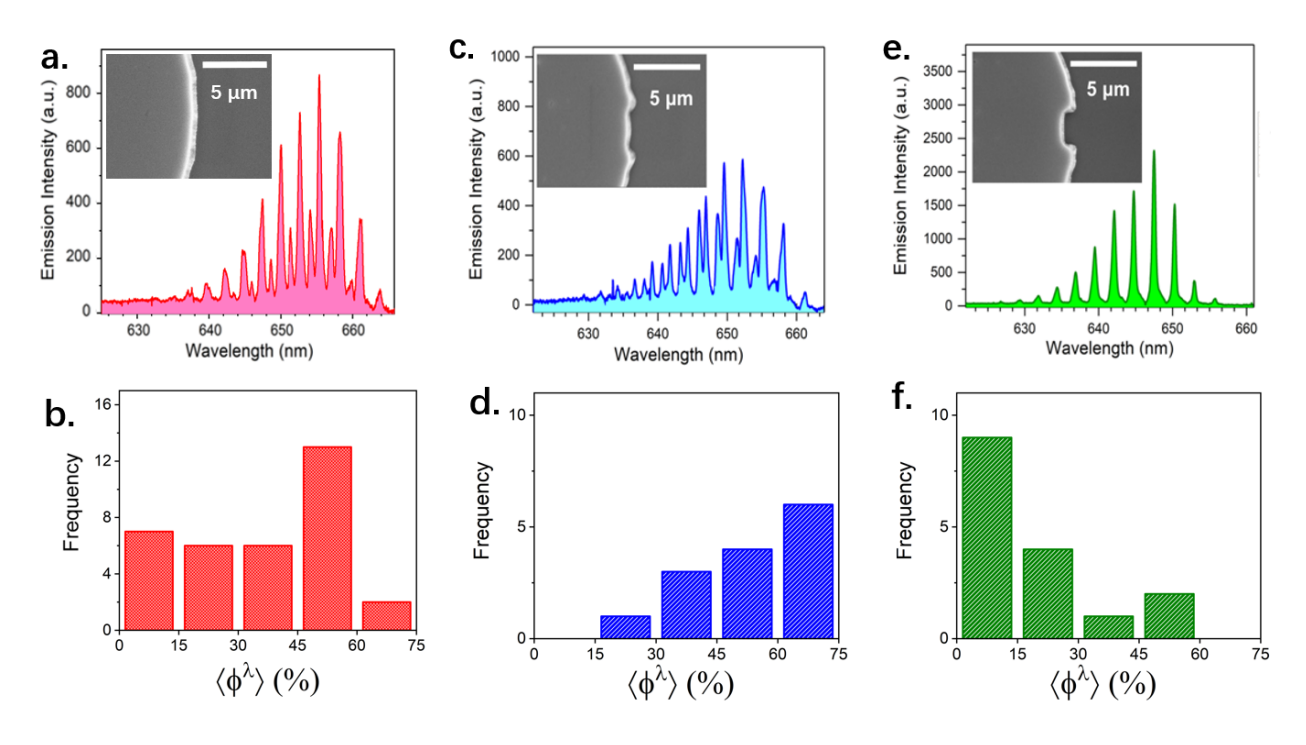


Figure 3. Spectral dependence of the notch depth. a. Typical emission spectrum of a pristine microdisk (no notch, as seen in the inset). b. Splitting parameter distribution of pristine microdisks. c. Typical emission spectrum of microdisk with an engineered notch depth d = 200 nm (SEM pictured in the inset). d. Splitting parameter distribution of small notch microdisks with d < 450 nm. e. Typical emission spectrum of microdisk with notch depth d = 1000 nm (SEM pictured in the inset). f. Splitting parameter distribution of microdisks with large notch ($d \ge 450$ nm) which consistently shows a strong reduction in mode splitting.

In order to further understand the effect of the engineered notch on the spectral properties of CQD microdisks, we also investigated structures with *two* engineered notches embedded in the circumference, for various values of notch depth. Figure 4b presents the spectrally integrated emission power as a function of notch depth. It can be seen that the power steeply decreases for d > 450 nm and that the microdisks remain below lasing threshold for d > 550 nm. The transition

from lasing to the absence of lasing in microdisks with two large notches is also apparent from the emission intensity observed along the circumference of the microdisks in the fluorescent images shown in Fig. 4b. For the disks containing two notches that show lasing modes, i.e. for $d \le 450$ nm the mode splitting of CW and CCW is generally observed (not shown here), similar to microdisks with a single small notch. We further confirmed that this was indeed due to the destruction of stable lasing modes rather than to strong redirection of outcoupling in any particular direction by measuring emission in the disk plane, which shows a similar emission power vs. notch depth dependence (not shown here).

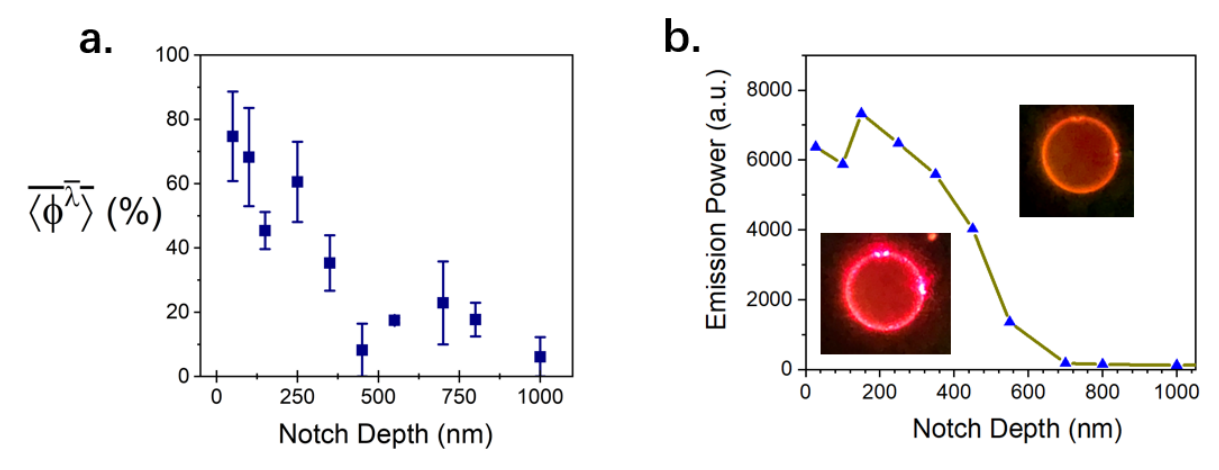


Figure 4. Notch depth dependence of laser mode splitting in single notch disks, and emission power of double notch disks. a. The laser modes splitting parameter averaged over several microdisks vs. engineered notch depth, d. b. Emission intensity vs. notch depth of microdisks with two engineered notch implantations. The insets show the fluorescent image of double notch disks with 400 nm (lower-left inset) and 1000 nm (upper-right) depth notches.

Our results confirm that the engineered notch dominates the spectral properties of WGMs in microdisk lasers. In such a laser cavity the frequency and amplitude of CW and CCW modes describe the eigenvalues and eigenfunctions of the system. The single notch breaks the degeneracy of the CW and CCW propagating modes, and instigates their mutual interaction leading to strong coupling with each other described by a coupling coefficient κ . This coupling results in the splitting of each mode as described by the mathematical frameworks of coupled-mode theory³⁹, where the eigenvalues of CW and CCW modes are described in equations (2a) and (2b), respectively,

$$\frac{da}{dt} = -j\omega_a a + j\kappa b + \gamma_a a \qquad (2a)$$

$$\frac{db}{dt} = -j\omega_b b + j\kappa a + \gamma_b b \qquad (2b)$$

where a and b represent the amplitudes of CW and CCW modes, ω_a and ω_b are the frequency of the modes, and γ_a and γ_b are the modal gain values which are directly related to the pump intensity. In the absence of coupling, $\omega_a = \omega_b = \omega_0$, and the CW and CCW modes are degenerate. When there is coupling, the eigenvalues of CW and CCW modes can be obtained by solving the coupled rate equations. We then obtain the eigenvalue equation (3)

$$\omega^{(a,b)} = \omega_0 + j \frac{\gamma_a + \gamma_b}{2} \pm \sqrt{\kappa^2 - (\frac{\gamma_a - \gamma_b}{2})^2}$$
 (3)

In this situation, CW and CCW form an interactive system. The frequency splitting can be expressed in the form $\omega^{(a,b)} = \omega_0 \pm \sqrt{\kappa^2 - \gamma^2}$, where γ is the gain-loss contrast between the coupled modes $\gamma = \gamma_a - \gamma_h$. When the notch depth is small, the gain-loss contrast γ of CW and CCW mode remains below the coupling coefficient κ ; consequently $\sqrt{\kappa^2 - \gamma^2}$ is real, and the eigenfrequencies of the two modes have the same imaginary part but show splitting in the real part, which represents the frequency splitting of the observed modes. As the depth of the notch increases, because of the phase difference of CW and CCW modes, the notch adds additional loss to one of the coupled WGMs, similar to the influence of nanoparticles on WGM modes as reported in Ref 8. The symmetric mode locates that notch at the antinode and the asymmetric mode locates the notch at the node, the symmetric mode experiences frequency shift and amplitude decay. When this additional loss is added to one of the CW and CCW modes, the gain-loss contrast γ increases. Consequently when γ exceeds κ , a conjugate pair of WGMs emerges. The eigenvalues of CW and CCW now share real frequency but have different modal gains. This can explain why the mode splitting disappears after a large notch is embedded in the microdisk. Furthermore, if a second notch with large depth is embedded in the microdisk, it will add additional loss to the surviving WGM, which will cause the net gain to remain below the threshold value for both CW and CCW modes, preventing the microdisk from lasing.

In our previous result²⁹, we found that the CW and CCW modes similarly form a strongly coupled lasing system in a microdisk laser with fabricated defects, and that coupling pairs of such microdisks results in the reduction of parasitic mode-splitting due to an exceptional point of the non-Hermitian system. The enhanced control over the influence of boundary perturbations imparted by controlled engineered notch defects provides an interesting expansion to the various phenomena that have been displayed in the non-Hermitian coupled WGM resonators^{30-35,40,41}. We have therefore subsequently investigated the coupling between two microdisks with engineered notches. For these measurements, the microdisk pair is swept through the pump beam spot incrementally. The offset between the pump spot and the pair center, which we call ΔD_p , then becomes a proxy for the gain/loss variation, between the two microdisks. In Figs. 5(a-c) we show the emission spectra obtained when a pair of microdisks each with d = 1000 nm notch is placed in the center of the laser beam, where $\Delta D_p = 0 \mu m$, so that both individual disks are pumped evenly (Fig. 5b), and when $\Delta D_p = \pm 25 \mu m$, the left and right disk are pumped exclusively (Figs. 5a,c). This latter configuration resembles the Parity-Time (PT) symmetric configuration³³. As discussed above, 1000 nm notch depth strongly reduces mode splitting between CW and CCW modes. When we pumped the notched microdisk individually, the emission spectra similarly do not show mode splitting since one of the CW and CCW diminishes due to their mutual interaction caused by the notch. In Fig. 5b both disks are pumped evenly, and the spectra show clear mode splitting. These results are consistent with the behavior of PT symmetry breaking^{33,40}. This phenomenon can also be explained using coupled-mode theory, similar to equations (2) above. With only one mode surviving in each disk due to the large notch, lasing modes of the two disks interact with each other with inter-disk coupling strength κ' . In this case, ω_L and ω_R are the frequency of the surviving modes in the left disk, L and the right disk, R, γ_L and γ_R is gain of left and right disk which is controlled by the spatial overlap of the pump beam spot and the microdisk pair.

$$\frac{dL}{dt} = -j\omega_L L + j\kappa' R + \gamma_L L \qquad (4a)$$

$$\frac{dR}{dt} = -j\omega_R R + j\kappa' L + \gamma_R R \qquad (4b)$$

After solving for eigenvalues, we get: $\omega^{(L,R)} = \omega_0 \pm \sqrt{\kappa'^2 - \gamma'^2}$. γ' is the gain-loss contrast between the coupled modes in left and right disks $\gamma_L - \gamma_R$. When left and right microdisks are pumped evenly (Fig. 5b), $\sqrt{\kappa'^2 - \gamma'^2} > 0$, thus the frequency splitting occurs in the real part of the eigenvalues and the spectra shows mode splitting. When either the left or right microdisk is pumped exclusively, γ' exceeds κ' , and thus $\sqrt{\kappa'^2 - \gamma'^2} < 0$, and both modes have same frequency but one of them is amplified and the other is attenuated. This causes the PT symmetry breaking and mode-splitting to not be observed in the emission spectra (Figs. 5a,c)

Quite a different situation occurs when we pump the disk pair with 200 nm depth notch. The emission spectrum of microdisk pair when the left and right disk are pumped individually show mode splitting (Figs. 5d,f). Again, we see the results from asymmetric pumping of the pair is similar to those of the individual disks, namely, mode splitting is observed because of the breaking of degeneracy of CW and CCW modes through their interaction with each other, which is caused by the engineered notch. Surprisingly, the emission spectrum of the evenly-pumped pair shows no trace of the mode-splitting (Fig. 5e). These results are similar to our previous report²⁹, which showed that mode splitting due to unintentional defects coalesce when both disks are equally pumped. In the current situation, there are four interacting modes; these are CW and CCW modes of the left and right disks. The CW mode in the left disk has stronger coupling strength to the CCW mode in the right disk than CW mode due to mutual directionality of propagation. For the same reason, the CCW mode in the left disk has stronger coupling strength to the CW mode in the right disk than the CCW mode. This generates a similar situation to that in Ref. 29, in which the existence of a large coupling anisotropy leads to coalescence of mode splitting when two disks are evenly pumped. The ability to realize these two distinct scenarios for evanescently coupled microdisk resonators is a direct consequence of the controlled intracavity coupling imparted by the notch. This demonstrates the ability of intracavity elements such as the engineered notch to tune interactions in PT-symmetric systems.

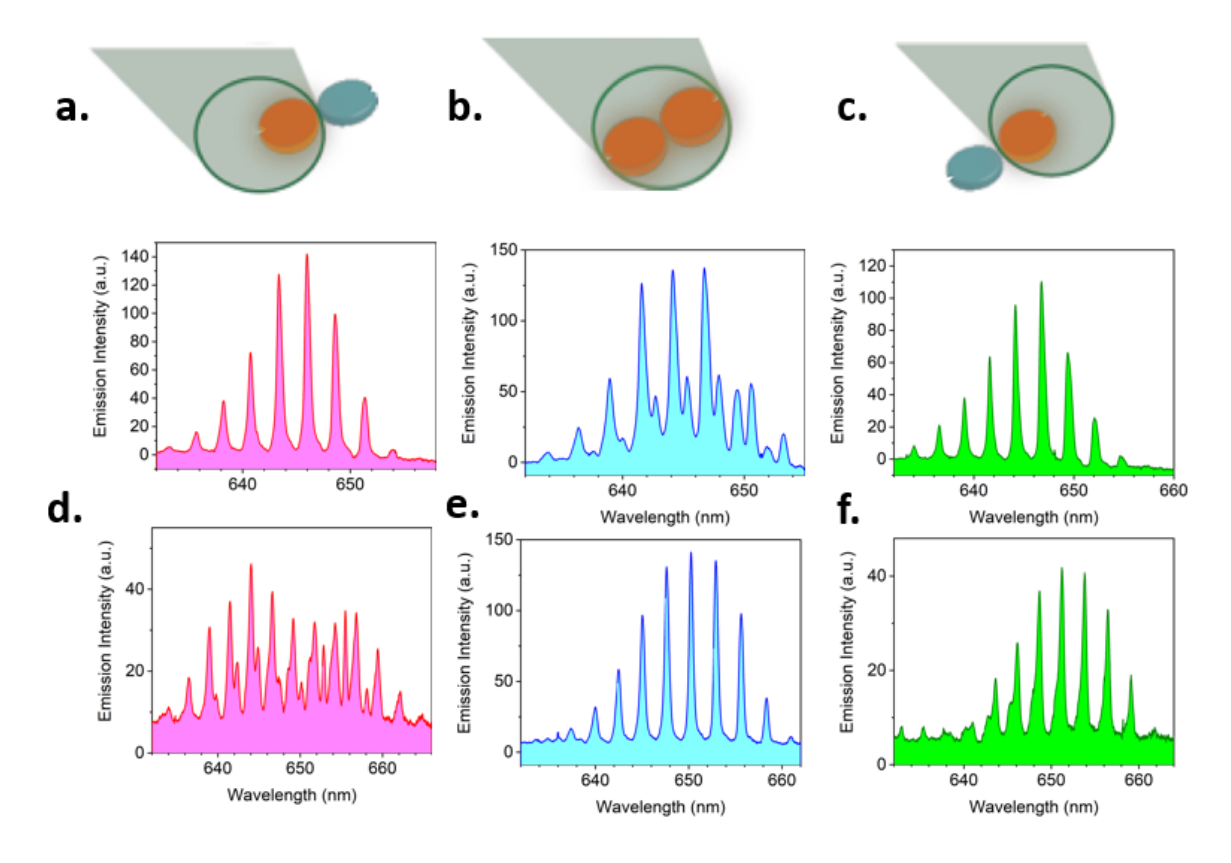


Figure 5. Laser emission characteristics of coupled pairs of microdisk resonators with engineered notch. a-c, Laser emission spectra from a coupled microdisk pair with 1000 nm depth engineered notch pumped in various configurations, where the pair is placed at different locations in the pump beam spot, such that only the left or right microdisk is pumped (a and c), or the pair is pumped evenly (b), as illustrated schematically above each plot. d-f, Laser emission spectra from a coupled microdisk pair with 200 nm depth engineered notch, pumped in the same configurations as in (a)-(c).

In order to provide direct experimental proof that the two scenarios described above result from the presence of exceptional points in the coupled systems, we show the behavior near the center of the beam spot as ΔD_p is varied incrementally. The results are displayed in Figure 6. For large notch depth of d=1000 nm (Fig. 6a,b), we observe a single set of WGM modes localized in one microdisk that begins to split when $\Delta D_p=-7.5~\mu m$. The splitting then increases as the pump beam moves closer to the center of the pair reaching a maximum near $\Delta D_p=0~\mu m$, where the gain/loss contrast is minimal. The splitting then decreases as ΔD_p increases, eventually coalescing into a single set of modes now localized in the other microdisk. For a smaller notch depth of d=200~nm, the opposite behavior is observed. In this case, the modes show broken degeneracy due to the presence of the engineered notch when the gain/loss contrast is high and the modes are localized. Then as ΔD_p approaches zero from either side, the modes move closer together before becoming indistinguishable and coalescing when the pump beam is placed at the center. The nature of the exceptional point in the coupled microdisk system is thus observed to be determined by the different kinds of intra-disk modal interactions provided by the depth of the engineered notch.

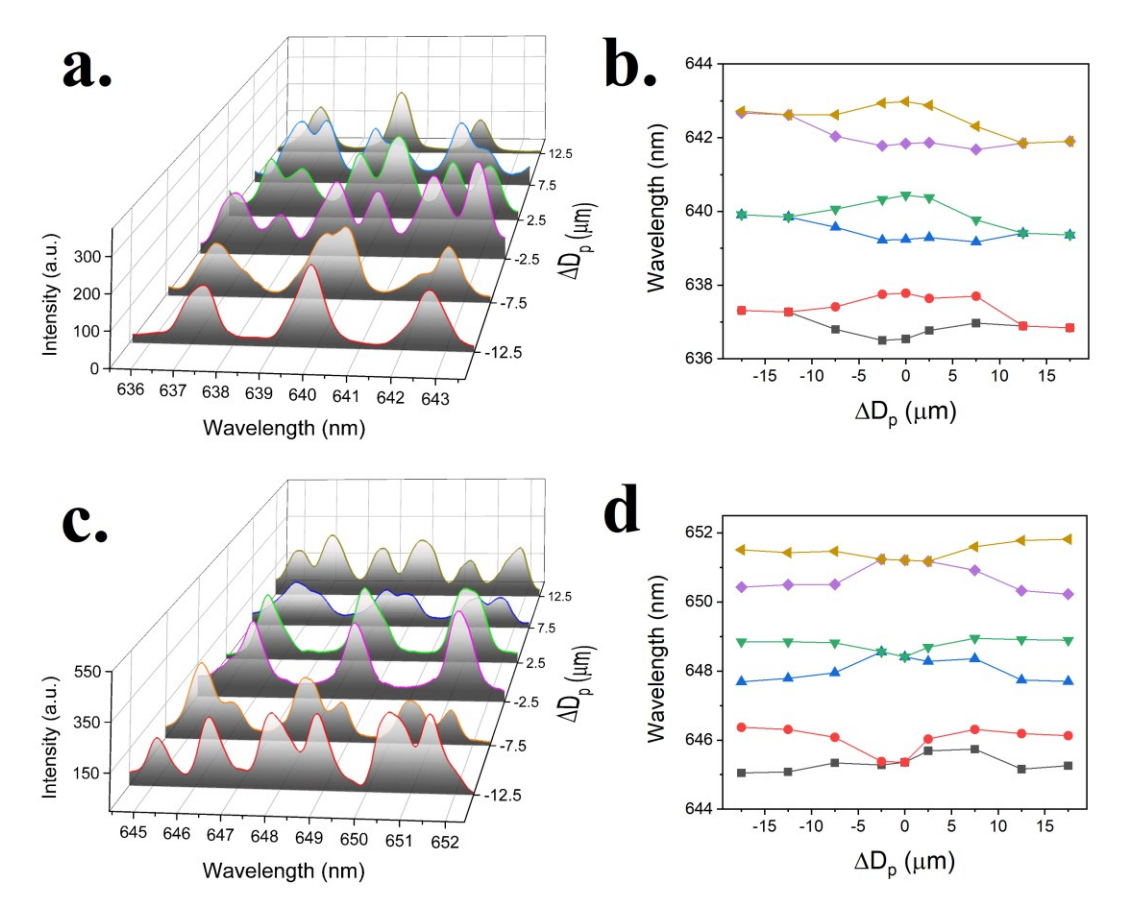


Figure 6. Modal behavior of coupled pairs of microdisk resonators in the vicinity of the exceptional point. a. Laser emission spectra from a coupled microdisk pair with 1000 nm depth engineered notch as a function of the overlap of the pump beam with the pair center, ΔDp . b. Positions of the mode peaks as a function of ΔDp . c, d. Same as (a,b) but for microdisk pairs containing engineered notch of 200nm depth.

Conclusion

By studying the lasing properties of microdisk cavities with engineered notches, we found that the implantation of a large engineered notch into the circular microdisk resonator diminishes the splitting between CC and CCW modes, as well as enhances the directionality of the resulting laser emission. In addition, it strongly diminishes the effects of natural fabrication defects and therefore can be a useful method for obtaining spectral purity in WGM resonators based on CQDs and other, less rigid materials. The engineered notch may thus be used to overcome roadblocks to the use of such low-cost flexible and chemically tunable materials that can expand the range of on-chip photonic applications. The role of the notch was described via the intracavity interaction of the counter propagating modes using coupled-mode theory. We further discussed the performance of these resonators in evanescently coupled pairs. Parity-Time symmetry breaking generated mode splitting due to inter-disk coupling when the external gain and loss contrast was modulated between microdisk pairs with large size notches, where mode splitting is quenched, while coalescence of mode splitting is achieved when disk pairs have small size notch and large coupling anisotropy between broken-degeneracy modes. The controlled intracavity mode interaction

provided an additional element of spectral control for tuning in inter-cavity coupled resonator non-Hermitian systems.

Supporting Information

Lithography based microfabrication process for CQD microdisks, Atomic Force Microscopy image of height profile of microdisks, Amplified Spontaneous Emission and threshold behavior of CQD thin film, Finite Difference Time Domain simulations of coupling rate and field profile between microdisks.

References

- 1. K. J. Vahala, "Optical Microcavities," *Nature* **424** 839-846 (2003).
- 2. V. V. Vassiliev, V. L. Velichansky, V. S. Ilchenko, M. L. Gorodetsky, L. Hollberg, and A. V. Yarovitsky, "Narrow-line-width diode laser with a high-Q microsphere," *Opt. Commun.* **158**, 305–312 (1998).
- 3. T. Le et al., "Low-threshold ultraviolet solid-state laser based on a Ce³⁺:LiCaAlF₆ crystal resonator," *Opt. Lett.* **37**, 4961-4963 (2012).
- 4. L. He, S K. Ozdemir, and L. Yang, "Whispering gallery microcavity lasers," *Laser Photonics Rev.* 7, 60-82 (2012).
- 5. M. L. Gorodetsky, A. A. Savchenkov, and V. S. Ilchenko, "Ultimate Q of optical microsphere resonators" *Opt. Lett.* **21**, 453–455 (1996).
- 6. D. K. Armani, T. J. Kippenberg, S. M. Spillane, and K. J. Vahala, "Ultra-high-Q toroid microcavity on a chip," *Nature* **421**, 925–928 (2003).
- 7. S. L. McCall, A. F. J. Levi, R. E. Slusher, S. J. Pearton, and R. A. Logan, "Whispering-gallery mode microdisk lasers," *Appl. Phys. Lett.* **60**, 289-291 (1992).
- 8. J. Zhu et al., "On-chip single nanoparticle detection and sizing by mode splitting in an ultrahigh-Q microresonator," *Nat. Photon.* **4**, 46–49 (2010).
- 9. P. Del'Haye, A. Schliesser, O. Arcizet, T. Wilken, R. Holzwarth, and T. J. Kippenberg, "Optical frequency comb generation from a monolithic microresonator," *Nature* **450**, 1214-1217 (2007).
- 10. M. A. Bandres et al., "Topological insulator laser: Experiments," *Science* **359**, eaar4005 (2018).
- 11. C. Gmachl et al., "High-Power Directional Emission from Microlasers with Chaotic Resonators," *Science* **280**, 1556-1564 (1998).
- 12. S. Lacey and H. Wang, "Directional emission from whispering-gallery modes in deformed fused-silica microspheres," *Opt. Lett.* **26**, 1943-1945 (2001).
- 13. R. Schäfer, U. Kuhl, and H.-J. Stöckmann, "Directed emission from a dielectric microwave billiard with quadrupolar shape," *New J. Phys.* **8**, 46 (2006).
- 14. T. Ben-Messaoud, and J. Zyss, "Unidirectional laser emission from polymer-based spiral microdisks," *Appl. Phys. Lett.* **86**, 241110 (2005).
- 15. R. C. Polson and Z. V. Vardeny, "Directional emission from asymmetric microlaser resonators of π -conjugated polymers," *Appl. Phys. Lett.* **85**, 1892–1894 (2004).
- 16. Q. J. Wang et al., "Whispering-gallery mode resonators for highly directional laser action," *Proc. Natl. Acad. Sci. U. S. A.* **107**, 22407–22412 (2010).
- 17. N. Gaponik, S. G. Hickey, D. Dorfs, A. L. Rogach, and A. Eychmüller, "Progress in the light

- emission of colloidal semiconductor nanocrystals," Small 6, 1364-1378 (2010).
- 18. C. H. Lin et al., "Large-scale robust quantum dot microdisk laser with controlled high quality cavity modes," *Adv. Opt. Mater.* **5**, 1700011 (2017).
- 19. S. Yakunin et al., "Low-threshold amplified spontaneous emission and lasing from colloidal nanocrystals of cesium lead halide perovskites," *Nat. Commun.* **6**, 8056, (2015).
- 20. J. Q. Grim, L. Manna, and I. Moreels, "A sustainable future for photonic colloidal nanocrystals," *Chem. Soc. Rev.* **44**, 5897-5914 (2015).
- 21. Y. Wang, S. Yang, H. Yang, and H. Sun, "Quaternary Alloy Quantum Dots: Toward Low-Threshold Stimulated Emission and All-Solution-Processed Lasers in the Green Region," *Adv. Opt. Mater.* **3**, 652-657 (2015).
- 22. M. M. Adachi et al., "Microsecond-sustained lasing from colloidal quantum dot solids," *Nat. Commun.* **6**, 8694 (2015).
- 23. Y. Wang et al., "Robust Whispering-Gallery Mode Microbubble Lasers from Colloidal Quantum Dots," *Nano Lett.* **17**, 2640-2646 (2017).
- 24. M. Kazes, D. Y. Lewis, Y. Ebenstein, T. Mokari, and U. Banin, "Lasing from Semiconductor Quantum Rods in a Cylindrical Microcavity," *Adv. Mater.* 14, 317-321 (2002).
- 25. C. Grivas et al., "Single-mode tunable laser emission in the single-exciton regime from colloidal nanocrystals," *Nat. Commun.* **4**, 2376 (2013).
- 26. B. Tang et al., "Single-Mode Lasers Based on Cesium Lead Halide Perovskite Submicron Spheres," *ACS Nano* **11**, 10681-10688 (2017).
- 27. M. Zavelani-Rossi, M. G. Lupo, R. Krahne, L. Manna, G. Lanzani, "Lasing in self-assembled microcavities of CdSe/CdS core/shell colloidal quantum rods," *Nanoscale* 2, 931-935 (2010).
- 28. M. Zavelani-Rossi et al., "Self-assembled CdSe/CdS nanorod micro-lasers fabricated from solution by capillary jet deposition," *Laser Photonics Rev.* **6**, 678-683 (2012).
- 29. E. Lafalce et al., "Robust lasing modes in coupled colloidal quantum dot microdisk pairs using a non-Hermitian exceptional point," *Nat. Commun.* **10**, 561 (2019).
- 30. R. El-Ganainy, K. G. Makris, M. Khajavikhan, Z.H. Musslimani, S. Rotter, and D. N. Christodoulides, "Non-Hermitian physics and PT symmetry," *Nat. Phys.* **14**, 11-19 (2018).
- 31. L. Feng, R. El-Ganainy, and L. Ge, "Non-Hermitian photonics based on parity-time symmetry," *Nat. Photon.* **11**, 752-762 (2017).
- 32. H. Hodaei, M.-A. Miri, M. Heinrich, D. N. Christodoulides, and M. Khajavikhan, "Parity-time-symmetric microring lasers," *Science* **346**, 975-978 (2014).
- 33. L. Feng, Z. J. Wong, R.-M. Ma, Y. Wang, and X. Zhang, "Single-mode laser by parity-time symmetry breaking," *Science* **346**, 972-975 (2014).
- 34. B. Peng et al., "Chiral modes and directional lasing at exceptional points," *Proc. Natl. Acad. Sci.* **113**, 6845-6850 (2016).
- 35. P. Miao et al., "Orbital angular momentum laser," Science 353, 464-467 (2016).
- 36. J. Jung et al., "Crafting Core/Graded Shell-Shell Quantum Dots with Suppressed Reabsorption and Tunable Stokes Shift as High Optical Gain Materials," *Angew. Chem, Int. Ed.* **55**, 5071-5075 (2016).
- 37. C. H. Lin et al., "Core/alloyed-shell quantum dot robust solid films with high optical gains," *ACS Photon.* **3**, 647-658 (2016).
- 38. S. T. Malak et al., "Enhancement of optical gain characteristics of quantum dot films by optimization of organic ligands," *J. Mater. Chem. C* 4, 10069-10081 (2016).
- 39. B. E. Little, S. T. Chu, H. A. Haus, J. Forsei, and J.-P. Laine, "Microring Resonator Channel Dropping Filters," J. *Lightwave Technol.* **15**, 998-1005 (1997).

- 40. M.-A. Miri, P. LiKamWa, and D. N. Christodoulides, "Large area single-mode parity-time symmetric laser amplifiers," *Opt. Lett.* **37**, 764-766 (2012).
- 41. B. Peng et al., "Parity-time-symmetric whispering-gallery microcavities," *Nat. Phys.* **10**, 394–398 (2014).
- 42. W. K. Bae, K. Char, H. Hur, and S. Lee, "Single-step synthesis of quantum dot with chemical composition gradients," *Chem. Mater.* **20**, 531-539 (2008).

Acknowledgements

This work was supported by the Air Force Office of Scientific Research (AFOSR) (MURI FA 9550-14-1-0037). C.H.L, Z.L. and V.V.T acknowledge supports for synthesis, fabrication and characterization of QD and photonic arrays from the Department of Energy (DOE) Office of Science (DE-SC0002232), Air Force Office for Scientific Research (AFOSR) (FA9550-16-1-0187 and FA9550-17-1-0297), and National Science Foundation (NSF) (NSF-CHE-1506046 and NSF-CBET-1803495). M. J. S. would like to acknowledge the Science, Mathematics and Research for Transformation (SMART) scholarship funded by OSD-T&E (Office of Secretary Defense-Test and Evaluation), Defense—Wide/PE0601120D8Z National Defense Education Program (NDEP)/BA-1, Basic Research, SMART Program office Grant Number N00244-09-1-0081.

Materials and Methods

Chemicals and Materials

Cadmium oxide, tri-n-octylphosphine (TOP, 90%), zinc acetate, dodecanethiol and selenium powder were obtained from Sigma Aldrich. 1-octadecene (ODE, 90%), butylamine (BA, 98%), oleic acid (OA, 97%), and sulfur were obtained from TCI. 1,7 diaminoheptane (DIAH, 98%) and ethyl lactate was obtained from Sigma Aldrich. Toluene and heptane were obtained from BDH Chemicals. CYTOP was obtained from AGC Chemicals. NR 71-3000p photoresist was purchased from Futurrex. All chemicals were used as received.

Synthesis of compositional gradient $CdSe/Cd_{1-x}Zn_xSe_{1-y}S_y$ QD

 $CdSe/Cd_{1-x}Zn_xSe_{1-y}S_y$ core/alloyed-shell QDs feature a CdSe core encased in a $Cd_{1-x}Zn_xSe_{1-y}S_y$ alloyed-shell, where x and y increase from zero at the shell interior to 1 at the shell outer-surface. These QDs were synthesized by modifying reported methods^{31,37}. The compositional gradient shell is created by using the reactivity difference between Cd, Zn, Se, and S precursors. Briefly, 1 mmol of CdO, 2 mmol of Zn(acetate)₂, 5 ml of oleic acid, and 15 ml of 1-octadecene (ODE) were placed in a three-neck flask and degassed at 150°C for 1 h. The reaction

was heated to 300°C under Ar. At the elevated temperature (300°C), 0.2 ml of 1M Se/TOP solution was rapidly injected to initiate nucleation and growth. After 5 min, 0.3 ml dodecanethiol was added. The reaction was kept at 300°C for 20 min. Then, 1 ml of 2M S/TOP was added. Then the heating mantle was removed to stop reaction. 10 ml of hexane was added to the solution once the temperature reached 70°C. The QD solution was purified by adding acetone as antisolvent to remove excess ligands. After discarding the supernatant, QDs were dissolved in heptane and stored in a refrigerator.

Microdisk Fabrication.

Fabrication of OD microdisks includes several steps. First, a low refractive index layer of CYTOP (n = 1.34) was deposited on the silicon wafer (n = 3.44) in order to provide light confinement within the QD cavities. CYTOP solution was spun cast on the substrate with a spin speed of 2500 rpm for 3 minutes. A subsequent baking at 100°C for 30 minutes was performed. This process was repeated two times to achieve film thickness of 1.5 µm. A short oxygen plasma etch (5 seconds) was performed to improve the wettability of the CYTOP surface for the deposition of the negative photoresist (NR 71-3000p). Ethyl lactate was added to the negative resist NR71-3000p solution to dilute it to one third of the original concentration provided by the company. The diluted resist was spun cast on the CYTOP/silicon substrate (3000 rpm for 1 minute). The cast film was subsequently soft baked at 165°C for 5 minutes and exposed to 365 nm with a dosage of 123 mW. The exposed film was then post-baked at 100°C for 5 minutes and developed by soaking in RD6 developer for 5 s. After the development, the film was rinsed with water and dried by blowing with air. The QD microdisks were fabricated by spin casting butylamine-capped QD solution (in heptane) of ~3-6 mg/mL at 1000 rpm for 1 minute onto the polymer pattern. The cast layer was subsequently immersed in 0.1M diaminoheptane solution in methanol for 1 minute and rinsed with methanol 2 times while spinning at 3000 rpm for 1 minute. The above process was repeated multiple times to achieve the desired thickness. The polymer pattern was subsequently removed by soaking in acetone while sonicating for 3-10 seconds. The characterization of gain properties of films was previously described³².

Scanning electron microscopy

SEM characterization was performed on a Hitachi S-3400N SEM with a back-scattering electron detector with an accelerating voltage in the range of 5-10 kV.

Optical Characterization.

The samples were placed on a three-dimensional stage under a home-built confocal microphotoluminescence set-up. The excitation source was provided by the second harmonic (532 nm) of a solid-state Nd:YAG laser delivering 7 ps pulses at a repetition rate of 200 Hz. The beam was focused through a 40x (NA = 0.65) microscope objective onto the sample using a dichroic mirror (550 nm long-pass). The emission from the sample was collected through the same objective, transmitted through the dichroic mirror as well as an additional 550 nm long-pass filter, focused onto a multimode optical fiber and recorded using a $\frac{1}{2}$ m spectrometer and CCD array. The spectral revolution of the setup was 0.2 nm. Alternatively, a camera was placed in the emission path to collect fluorescent images of the microdisks. The beam size was set with an iris to 50 μ m in diameter.

For TOC only

